

Measurement of $B_s^0 \rightarrow D_s^{(*)+} D_s^{(*)-}$ Branching Ratios

(Dated: February 22, 2012)

Abstract

The decays $B_s^0 \rightarrow D_s^{(*)+} D_s^{(*)-}$ are reconstructed in a data sample corresponding to an integrated luminosity of 6.8 fb^{-1} collected by the CDF II detector at the Tevatron $p\bar{p}$ collider. The $B_s^0 \rightarrow D_s^{*+} D_s^{*-}$ decay is observed for the first time with a significance of more than 10σ , and we measure the B_s^0 production rate times $B_s^0 \rightarrow D_s^{(*)+} D_s^{(*)-}$ branching ratios relative to the normalization mode $B^0 \rightarrow D_s^+ D^-$ to be $0.183 \pm 0.021 \pm 0.017$ for $B_s^0 \rightarrow D_s^+ D_s^-$, $0.424 \pm 0.046 \pm 0.035$ for $B_s^0 \rightarrow D_s^{*\pm} D_s^\mp$, $0.654 \pm 0.072 \pm 0.065$ for $B_s^0 \rightarrow D_s^{*+} D_s^{*-}$, and $1.261 \pm 0.095 \pm 0.112$ for the inclusive decay $B_s^0 \rightarrow D_s^{(*)+} D_s^{(*)-}$, where the uncertainties are statistical and systematic. These results are the most precise single measurements to date and provide important constraints for indirect searches for non standard model physics in B_s^0 mixing.

PACS numbers: 13.25.Hw, 14.40.Nd, 12.15.Nf

14 A B_s^0 meson can oscillate into its antiparticle via second order weak interaction transi-
 15 tions, which make its time evolution sensitive to contributions from new physics processes.
 16 Such contributions are not well constrained yet and might be responsible for the deviation
 17 from the standard model reported in Ref. [1]. The B_s^0 eigenstates with defined mass and
 18 lifetime, B_{sL}^0 and B_{sH}^0 , are linear combinations of the B_s^0 and \bar{B}_s^0 states and, in the standard
 19 model, correspond in good approximation to the even and odd CP eigenstates, respectively.
 20 In the absence of substantial CP violation, a sizable decay width difference between the light
 21 and heavy mass eigenstates, $\Delta\Gamma_s = \Gamma_{sL} - \Gamma_{sH}$, arises from the fact that decays to final states
 22 of definite CP are only accessible by one of the mass eigenstates. The dominant contribution
 23 to $\Delta\Gamma_s$ is believed to come from the $B_s^0 \rightarrow D_s^{(*)+} D_s^{(*)-}$ decays [2], which are predominantly
 24 CP -even and saturate $\Delta\Gamma_s$ under certain theoretical assumptions [3, 4], resulting in the
 25 relation

$$2\mathcal{B}(B_s^0 \rightarrow D_s^{(*)+} D_s^{(*)-}) \approx \frac{\Delta\Gamma_s}{\Gamma_s + \Delta\Gamma_s/2}, \quad (1)$$

26 where $\Gamma_s = (\Gamma_{sL} + \Gamma_{sH})/2$. However, three-body modes may provide a significant contribu-
 27 tion to $\Delta\Gamma_s$ [5].

28 A finite value of $\Delta\Gamma_s$ improves the experimental sensitivity to CP violation because
 29 it allows one to distinguish the two mass eigenstates via their decay time distribution.
 30 Furthermore, the $B_s^0 \rightarrow D_s^{(*)+} D_s^{(*)-}$ decays could be used in future to measure directly the
 31 lifetime of the CP -even eigenstate, which would complement the CP -odd eigenstate lifetime
 32 measurement in $B_s^0 \rightarrow J/\psi f_0(980)$ decays [6] and provide additional information in the
 33 search for new physics contributions to CP violation in the B_s^0 system.

34 The $B_s^0 \rightarrow D_s^{(*)+} D_s^{(*)-}$ decay modes have been previously studied by the ALEPH, CDF,
 35 D0, and Belle collaborations [7–10]. The current world average branching ratios [11],
 36 which do not yet include the latest preliminary Belle results [12], are $\mathcal{B}(B_s^0 \rightarrow D_s^+ D_s^-) =$
 37 $(1.04_{-0.26}^{+0.29})\%$, $\mathcal{B}(B_s^0 \rightarrow D_s^{*\pm} D_s^\mp) = (2.8 \pm 1.0)\%$, $\mathcal{B}(B_s^0 \rightarrow D_s^{*+} D_s^{*-}) = (3.1 \pm 1.4)\%$, and
 38 $\mathcal{B}(B_s^0 \rightarrow D_s^{(*)+} D_s^{(*)-}) = (4.5 \pm 1.4)\%$.

39 In a data sample corresponding to an integrated luminosity of 6.8 fb^{-1} recorded by the
 40 CDF II detector at the Tevatron $p\bar{p}$ collider we reconstruct $B_s^0 \rightarrow D_s^{(*)+} D_s^{(*)-}$ decays with
 41 $D_s^+ \rightarrow K^+ K^- \pi^+$. For the first time in this channel, the acceptance is calculated using a D_s^\pm
 42 Dalitz model instead of a simple two-body decay model. The photon and the neutral pion
 43 from the $D_s^{*+} \rightarrow D_s^+ \gamma$ and $D_s^{*+} \rightarrow D_s^+ \pi^0$ decays are not reconstructed because of their low

44 detection efficiency. In a simultaneous fit to the reconstructed $B_{(s)}^0$ meson invariant mass
 45 spectra we measure the B_s^0 production rate times $B_s^0 \rightarrow D_s^{(*)+} D_s^{(*)-}$ branching ratios relative
 46 to the normalization mode $B^0 \rightarrow D_s^+ D^-$

$$f_X = \frac{f_s}{f_d} \frac{\mathcal{B}(B_s^0 \rightarrow X)}{\mathcal{B}(B^0 \rightarrow D_s^+ D^-)}, \quad (2)$$

47 for $X = D_s^+ D_s^-$, $D_s^{*\pm} D_s^\mp$, $D_s^{*+} D_s^{*-}$, and $D_s^{(*)+} D_s^{(*)-}$ where f_s/f_d is the relative rate of
 48 produced B_s^0 to B^0 mesons.

49 The components of the CDF II detector [13] most relevant for this analysis are the tracking
 50 systems located inside a solenoid that provides a 1.4 T magnetic field. Charged particles'
 51 trajectories (tracks) are reconstructed in layers of silicon-strip sensors located between radii
 52 of 1.5 cm and 28 cm from the beam line and an open-cell drift chamber (COT) with a
 53 radial extension from 40 to 137 cm. Tracks with a pseudorapidity $|\eta| \leq 1.0$ pass the full
 54 radial extent of the COT. Kaons and pions are statistically identified by measurements
 55 of the ionization energy loss in the COT and information from the time-of-flight system
 56 located between the COT and the solenoid. The events for this analysis are selected online
 57 by identifying pairs of tracks detected in the COT and the silicon detector [14]. Minimal
 58 requirements on the momenta and the displacement of the tracks and the reconstructed
 59 decay vertex from the primary vertex are imposed.

60 We reconstruct $D_s^+ \rightarrow K^+ K^- \pi^+$ and $D^+ \rightarrow K^- \pi^+ \pi^+$ decays from combinations of
 61 three tracks with appropriate charge and mass hypothesis assignments, fitted to a common
 62 vertex. Because the $D_s^+ \rightarrow K^+ K^- \pi^+$ decay proceeds mainly via $\phi \pi^+$ and $\bar{K}^{*0} K^+$, we
 63 select candidates with $1.005 < m(K^+ K^-) < 1.035$ GeV/ c^2 and $0.837 < m(K^- \pi^+) < 0.947$
 64 GeV/ c^2 , centered on the known ϕ and K^{*0} masses, respectively. According to the $D_s^+ \rightarrow$
 65 $K^+ K^- \pi^+$ Dalitz structure [15] this requirement has a signal acceptance of $\sim 75\%$ while
 66 covering only 14% of the phase space and thus increasing the signal-to-background ratio.
 67 In the following we will denote the selected $K^+ K^-$ and $K^- \pi^+$ combinations as ϕ and \bar{K}^{*0} ,
 68 respectively, since the dominant contributions come from these resonances. However, we
 69 implicitly include contributions from other resonances and interference effects when using
 70 these terms.

71 Pairs of $D_s^+ \rightarrow \phi \pi^+$ or $D_s^+ \rightarrow \bar{K}^{*0} K^+$ candidates and $D_s^- \rightarrow \phi \pi^-$ candidates are combined
 72 to form B_s^0 candidates and fitted to a common vertex. Combinations where both charm
 73 mesons decay into a \bar{K}^{*0} mode are not considered because of the low signal-to-background

ratio. Candidate B^0 mesons are reconstructed from $D_s^+ D^-$ combinations where both D_s^+ decay modes are used.

To reject background-like events, requirements are placed on track quality variables, B meson momentum, reconstructed D meson masses, vertex fit qualities, and vertex displacement significances. To further increase the signal purity, two artificial neural networks are used, one for candidates with a \bar{K}^{*0} and one for candidates without. To minimize the systematic uncertainty of the relative selection efficiency, the same networks are applied to B_s^0 and B^0 candidates, and only information from the D_s^\pm that is common to both B meson decays is used. The networks are trained on simulated signal events, described below, and on background events from the 5.45 to 6.5 GeV/ c^2 B mass sideband. The input variables contain kinematic, lifetime, fit quality, and particle identification information. The B vertex displacement significance in the transverse plane gives the largest contribution to the discrimination power of both networks. The selection criteria on the network outputs are chosen such that they maximize the significance $\epsilon_{\text{MC}}/\sqrt{N_{\text{data}}}$, where ϵ_{MC} is the B_s^0 selection efficiency determined from simulation and N_{data} is the number of data events in the B_s^0 signal window from 5.343 to 5.397 GeV/ c^2 .

About 6 % of the selected $B^0 \rightarrow D_s^+(\rightarrow \phi\pi^+)D^-$ candidates also fulfill the B_s^0 selection requirements, where the assignment of a D^- daughter track is swapped from pion to kaon. To avoid having the same event entering the fit multiple times, we reject each event that is reconstructed as B_s^0 candidates from the B^0 sample. The cross-populations between the two B_s^0 modes and between the two B^0 modes, respectively, are negligible. The selected sample contains about 750 B_s^0 signal events.

Simulated events are used to determine the reconstruction and selection efficiency. The $B_{(s)}^0$ mesons are generated according to the momentum spectrum measured in exclusive B decays and decayed to the considered final states with the EVTGEN package [16]. For the B_s^0 meson we assign the lifetime of the B_{sL}^0 eigenstate [11] that coincides with the CP -even eigenstate in the standard model. For all the other long-lived charm and bottom mesons, the world average mean lifetimes [11] are used. The $B_s^0 \rightarrow D_s^{*+} D_s^{*-}$ decay is a transition of a scalar to two vector mesons and its angular distribution is described by three polarization amplitudes. Since these amplitudes are unknown, we take the same longitudinal polarization as measured in $B^0 \rightarrow D^{*+} D^{*-}$ decays [17] and a vanishing CP -odd component as default values. The world average value [11] is used for the ratio of $D_s^{*+} \rightarrow D_s^+ \gamma$ to $D_s^{*+} \rightarrow D_s^+ \pi^0$

106 decays. The dynamics of the decay $D_s^+ \rightarrow K^+ K^- \pi^+$ is simulated according to the Dalitz
 107 structure measured by CLEO [15]. The generated events are processed by a GEANT3 based
 108 detector simulation [18] and the same reconstruction program as applied to real data events.

109 The relative branching ratios times production rate are determined in a simultaneous ex-
 110 tended unbinned maximum-likelihood fit to the $(\phi\pi^+)(\phi\pi^-)$, $(\bar{K}^{*0}K^+)(\phi\pi^-)$, $(\phi\pi^+)(K^+\pi^-\pi^-)$,
 111 and $(\bar{K}^{*0}K^+)(K^+\pi^-\pi^-)$ invariant mass distributions. By simultaneously fitting all four
 112 distributions the normalization of the B^0 reflections in the $(\bar{K}^{*0}K^+)(\phi\pi^-)$ spectrum is con-
 113 strained by the yields in the high-statistics $(\phi\pi^+)(K^+\pi^-\pi^-)$ sample. The components of the
 114 fit function for each invariant mass distribution are fully and partially reconstructed signals,
 115 reflections, and background. The fully reconstructed B_s^0 and B^0 signals are parametrized by
 116 the sum of two Gaussians with relative normalizations and widths taken from simulation. To
 117 account for discrepancies between data and simulation, a factor is introduced for the B_s^0 and
 118 B^0 signal shapes, respectively, that scales the widths of the Gaussians and that is allowed
 119 to float in the fit. The shapes of partially reconstructed signal events and of reflections from
 120 $B^0 \rightarrow (\phi\pi^+)(K^+\pi^-\pi^-)$ mis-reconstructed as $B_s^0 \rightarrow (\phi\pi^+)(K^{*0}K^-)$ are determined from
 121 simulation using empirical models. Background from random combinations of tracks and
 122 other B decays is described by an exponential plus a constant function with all parameters
 123 floated in the fit.

124 The yield of fully reconstructed B^0 mesons in the final state i , $(\phi\pi^+)(K^+\pi^-\pi^-)$ or
 125 $(\bar{K}^{*0}K^+)(K^+\pi^-\pi^-)$, is given by

$$N_{\text{rec},i}^{B^0} = N_{\text{tot}}^{B^0} \mathcal{B}(B^0 \rightarrow D_s^+ D^-) \mathcal{B}(D_s^+ \rightarrow K^+ K^- \pi^+) \mathcal{B}(D^+ \rightarrow K^- \pi^+ \pi^+) \epsilon_i^{B^0}, \quad (3)$$

126 where $N_{\text{tot}}^{B^0}$ is the total number of produced B^0 mesons and is a free parameter in the fit,
 127 the branching ratios are taken from Ref. [11], and the efficiency $\epsilon_i^{B^0}$ is determined from
 128 simulation. Equivalent formulas are used for the yields of partially reconstructed B^0 decays
 129 with an additional branching ratio factor for the D^{*+} and D_s^{*+} decays. The normalizations
 130 of reflections are calculated in the same way, but with the efficiencies replaced by the mis-
 131 reconstruction fractions determined from simulation. The number of fully reconstructed B_s^0
 132 mesons in the final state i , $(\phi\pi^+)(\phi\pi^-)$ or $(\bar{K}^{*0}K^+)(\phi\pi^-)$, where the D_s^+ decays in the same

mode as the D_s^+ from the B^0 decay is given by

$$N_{\text{rec},i}^{B_s^0} = N_{\text{rec},i}^{B^0} f_{D_s D_s} \frac{\mathcal{B}(D_s^+ \rightarrow K^+ K^- \pi^+) \epsilon_i^{B_s^0}}{\mathcal{B}(D^+ \rightarrow K^- \pi^+ \pi^+) \epsilon_i^{B^0}}, \quad (4)$$

with $f_{D_s D_s}$ as a free parameter and $N_{\text{rec},i}^{B^0}$ given by Eq. (3). Equivalent equations hold for partially reconstructed B_s^0 decays.

Projections of the fit result are compared to the distribution of data events in Fig. 1. The statistical significance of each signal exceeds 10σ as estimated from a likelihood ratio of the fit with and without the signal component.

Systematic uncertainties on the fitted signal yields arise from the signal and background models. Because the width scale factors of the fully reconstructed signal components are allowed to float in the fit, the systematic uncertainties of these components are already included in the statistical errors. To estimate the systematic effect due to the fixed shapes of the partially reconstructed signal components and reflections, we repeat the fit multiple times with shape parameters randomly varied according to the covariance matrix of the fits of the shapes to simulated data. The mean deviations with respect to the central values are assigned as systematic uncertainties. The systematic uncertainties due to the background mass model are estimated from the changes in the results caused by using a 2nd order polynomial instead of the sum of an exponential and a constant function. By applying the selection optimization procedure on the normalization instead of the signal mode we verified that a possible selection bias is negligible.

Systematic effects in the relative efficiency determination can be caused by a simulation that does not describe the data accurately. One source of systematic uncertainties is the trigger simulation, which can lead to a discrepancy in the B meson momentum spectrum. Although this effect cancels to first order in the ratio measurement, it is accounted for by a reweighting of the simulated events. The systematic uncertainties due to the detector simulation are estimated by the shift of the results with respect to the case in which this reweighting is not applied. The uncertainties on the world average B^0 , D^+ , and D_s^+ lifetimes are propagated by varying the lifetimes in the simulation. For the B_s^0 lifetime, we consider two cases, the 1σ lower bound of the world average short-lived eigenstate lifetime and the 1σ upper bound of the mean B_s^0 lifetime. The effects on the acceptance induced by variations of the $D_s^+ \rightarrow K^+ K^- \pi^+$ Dalitz structure are considered by generating different Dalitz model scenarios, with Dalitz model parameter values varied according to the systematic and cor-

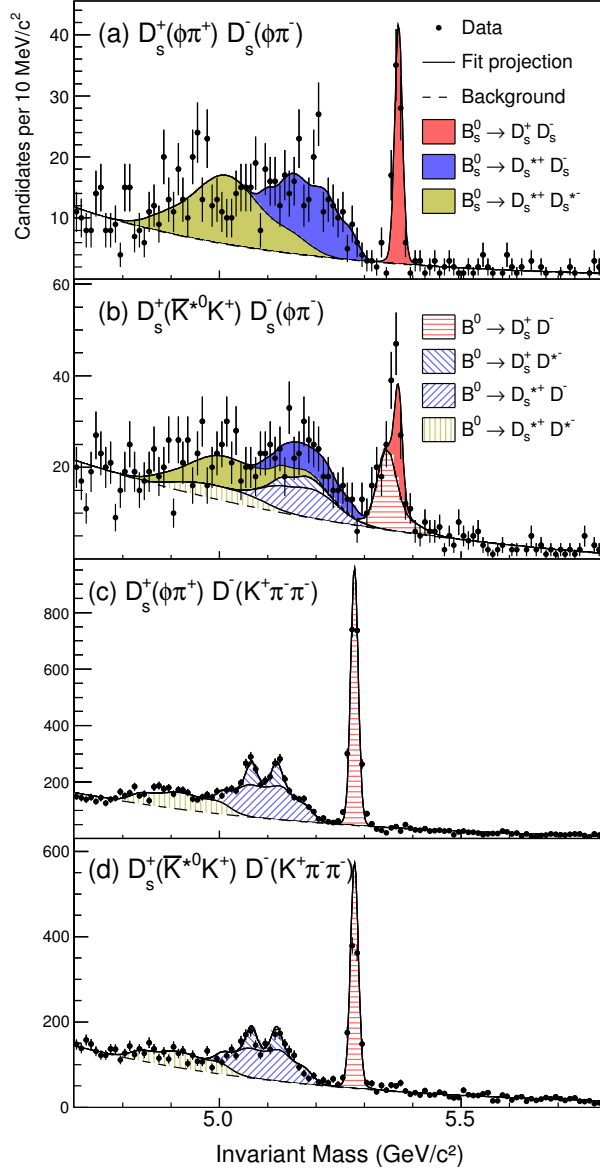


FIG. 1. Invariant mass distribution of (a) $B_s^0 \rightarrow D_s^+(\phi\pi^+)D_s^-(\phi\pi^-)$, (b) $B_s^0 \rightarrow D_s^+(\bar{K}^{*0}K^+)D_s^-(\phi\pi^-)$, (c) $B^0 \rightarrow D_s^+(\phi\pi^+)D^-(K^+\pi^-\pi^-)$, and (d) $B^0 \rightarrow D_s^+(\bar{K}^{*0}K^+)D^-(K^+\pi^-\pi^-)$ candidates with the simultaneous fit projection overlaid. The broader structures stem from decays where the photon or π^0 from the $D_{(s)}^{*+}$ decay is not reconstructed. Misreconstructed signal events in (c) show up as reflections in (b).

related statistical uncertainties of the CLEO Dalitz fit. The uncertainties of the D^+ Dalitz model have a negligible effect on the result. For $B_s^0 \rightarrow D_s^{*+}D_s^{*-}$ decays we investigate the effects of both a longitudinal polarization fraction f_L deviating from our nominal assumption

Source	$f_{D_s D_s}$	$f_{D_s^* D_s}$	$f_{D_s^* D_s^*}$	$f_{D_s^{(*)} D_s^{(*)}}$
Signal Model	0.003	0.007	0.009	0.019
Background Model	0.001	0.004	0.030	0.033
Detector Simulation	0.001	0.003	0.010	0.005
B, D Lifetimes	$+0.001$ -0.002	$+0.002$ -0.004	$+0.003$ -0.006	$+0.006$ -0.012
Dalitz Model	0.011	0.024	0.038	0.073
Helicity Model	0.001	0.005	0.012	0.008
Branching Fractions	0.013	0.024	0.039	0.074
Total	0.017	0.035	0.065	0.112

TABLE I. Overview of systematic uncertainties on the measured ratios of branching fractions.

tion and a non-zero fraction of the CP -odd component f_{CP-} . The fraction f_L is varied in the simulation according to the uncertainty of the f_L measurement in $B^0 \rightarrow D^{*+} D^{*-}$ decays [17]. A variation of f_{CP-} shows no effect on the $B_s^0 \rightarrow D_s^{*+} D_s^{*-}$ mass line shape, fit quality, or measured branching fraction ratios. The effect of self cross-feed due to a wrong assignment of kaon and pion masses is negligible.

Further systematic uncertainties arise from external input quantities. The uncertainties of intermediate and final state branching fractions, $\mathcal{B}(D_s^+ \rightarrow K^+ K^- \pi^+)$, $\mathcal{B}(D^+ \rightarrow K^- \pi^+ \pi^+)$, and $\mathcal{B}(D^{*+} \rightarrow D^+ \gamma / \pi^0)$, are propagated in the fit by adding Gaussian constraints to the corresponding fit parameters. The resulting uncertainties of the measured branching fraction ratios are extracted by subtracting in quadrature the statistical uncertainties of the fits with branching fraction constrained and the one where they are fixed to the central values. When calculating the absolute branching fractions $\mathcal{B}(B_s^0 \rightarrow D_s^{(*)+} D_s^{(*)-})$ an additional relative uncertainty of 16% is introduced by the measurement uncertainties of f_s/f_d and the branching fraction of the normalization channel $B^0 \rightarrow D_s^+ D^-$. The systematic uncertainties are summarized in Table I.

As a result we obtain $f_{D_s D_s} = 0.183 \pm 0.021 \pm 0.017$, $f_{D_s^* D_s} = 0.424 \pm 0.046 \pm 0.035$, $f_{D_s^* D_s^*} = 0.654 \pm 0.072 \pm 0.065$, and $f_{D_s^{(*)} D_s^{(*)}} = 1.261 \pm 0.095 \pm 0.112$, where the first uncertainties are statistical and the second systematic. Taking $\mathcal{B}(B^0 \rightarrow D_s^+ D^-) = (7.2 \pm 0.8) \times 10^{-3}$ from Ref. [11] and $f_s/f_d = 0.269 \pm 0.033$ from Ref. [11, 19] an absolute inclusive branching ratio of $\mathcal{B}(B_s^0 \rightarrow D_s^{(*)+} D_s^{(*)-}) = (3.38 \pm 0.25 \pm 0.30 \pm 0.56)\%$ is calculated where the third

uncertainty comes from the normalization. Assuming Eq. (1) to hold this would translate into a decay width difference contribution of the $B_s^0 \rightarrow D_s^{(*)+} D_s^{(*)-}$ modes of $\Delta\Gamma_s/\Gamma_s = (6.99 \pm 0.54 \pm 0.64 \pm 1.20) \%$.

In summary, we have measured the branching ratios of $B_s^0 \rightarrow D_s^+ D_s^-$, $B_s^0 \rightarrow D_s^{*\pm} D_s^\mp$, $B_s^0 \rightarrow D_s^{*+} D_s^{*-}$, and $B_s^0 \rightarrow D_s^{(*)+} D_s^{(*)-}$ decays relative to the normalization mode $B^0 \rightarrow D_s^+ D^-$. The decay $B_s^0 \rightarrow D_s^{*+} D_s^{*-}$ is observed for the first time. Compared to previous analyses, we have reduced the systematic uncertainties by taking into account the full $D_s^+ \rightarrow K^+ K^- \pi^+$ Dalitz structure, as opposed to using a simple two-body D_s^+ decay model. The derived absolute branching ratios of $\mathcal{B}(B_s^0 \rightarrow D_s^+ D_s^-) = (0.49 \pm 0.06 \pm 0.05 \pm 0.08) \%$, $\mathcal{B}(B_s^0 \rightarrow D_s^{*\pm} D_s^\mp) = (1.13 \pm 0.12 \pm 0.09 \pm 0.19) \%$, $\mathcal{B}(B_s^0 \rightarrow D_s^{*+} D_s^{*-}) = (1.75 \pm 0.19 \pm 0.17 \pm 0.29) \%$, and $\mathcal{B}(B_s^0 \rightarrow D_s^{(*)+} D_s^{(*)-}) = (3.38 \pm 0.25 \pm 0.30 \pm 0.56) \%$, where the uncertainties are statistical, systematic, and due to the normalization, are the most precise measurements to date. The central values are lower than but consistent with the Belle result [10] and the previous CDF result, which is superseded by this measurement.

We thank Mikhail S. Dubrovin and David Cinabro for their help in implementing the CLEO Dalitz model. We thank the Fermilab staff and the technical staffs of the participating institutions for their vital contributions. This work was supported by the U.S. Department of Energy and National Science Foundation; the Italian Istituto Nazionale di Fisica Nucleare; the Ministry of Education, Culture, Sports, Science and Technology of Japan; the Natural Sciences and Engineering Research Council of Canada; the National Science Council of the Republic of China; the Swiss National Science Foundation; the A.P. Sloan Foundation; the Bundesministerium für Bildung und Forschung, Germany; the Korean World Class University Program, the National Research Foundation of Korea; the Science and Technology Facilities Council and the Royal Society, UK; the Russian Foundation for Basic Research; the Ministerio de Ciencia e Innovación, and Programa Consolider-Ingenio 2010, Spain; the Slovak R&D Agency; the Academy of Finland; and the Australian Research Council (ARC).

[1] V. M. Abazov *et al.* (D0 Collaboration), Phys. Rev. D **84**, 052007 (2011).

[2] Charge-conjugate modes are implicitly included throughout this paper.

- 215 [3] R. Aleksan *et al.*, Phys. Lett. B **316**, 567 (1993).
- 216 [4] M. A. Shifman and M. B. Voloshin, Yad. Fiz. **47**, 801 (1988) [Sov. J. Nucl. Phys. **47**, 511
217 (1988)].
- 218 [5] C. K. Chua, W. S. Hou, and C. H. Shen, Phys. Rev. D **84**, 074037 (2011).
- 219 [6] T. Aaltonen *et al.* (CDF Collaboration), Phys. Rev. D **84**, 052012 (2011).
- 220 [7] R. Barate *et al.* (ALEPH Collaboration), Phys. Lett. B **486**, 286 (2000).
- 221 [8] T. Aaltonen *et al.* (CDF Collaboration), Phys. Rev. Lett. **100**, 021803 (2008).
- 222 [9] V. M. Abazov *et al.* (D0 Collaboration), Phys. Rev. Lett. **102**, 091801 (2009).
- 223 [10] S. Esen *et al.* (Belle Collaboration), Phys. Rev. Lett. **105**, 201802 (2010).
- 224 [11] K. Nakamura *et al.* (Particle Data Group), J. Phys. G **37**, 075021 (2010), and 2011 partial
225 update.
- 226 [12] S. Esen, arXiv:hep-ex/1110.2099.
- 227 [13] D. E. Acosta *et al.* (CDF Collaboration), Phys. Rev. D **71**, 032001 (2005).
- 228 [14] E. J. Thomson *et al.*, IEEE Trans. Nucl. Sci., **49**, 1063 (2002); B. Ashmanskas *et al.*, Nucl.
229 Instrum. Methods A **518**, 532 (2004); L. Ristori and G. Punzi, Ann. Rev. Nucl. Part. Sci **60**,
230 595 (2010).
- 231 [15] R. E. Mitchell *et al.* (CLEO Collaboration), Phys. Rev. D **79**, 072008 (2009).
- 232 [16] D. Lange, Nucl. Instrum. Methods A **462**, 152 (2001).
- 233 [17] B. Aubert *et al.* (BaBar Collaboration), Phys. Rev. D **67**, 092003 (2003).
- 234 [18] R. Brun, R. Hagelberg, M. Hansroul, and J. Lassalle, CERN-DD-78-2-REV, 1978 (unpub-
235 lished).
- 236 [19] T. Aaltonen *et al.* (CDF Collaboration), Phys. Rev. D **77**, 072003 (2008).